



Research Article

Thermo-Diffusion Effects on Fractional Ordered Model of Unsteady Casson Blood Flow with Magnetic Field Effect

Nilesh Patel¹, Harshad Patel^{2*}

¹Gujarat Technological University, Ahmedabad, Gujarat, India

²U.V. Patel College of Engineering, Vadodara (UVPCE), Ganpat University, 384 012 Gujarat, India
Email: harshadpatel2@gmail.com

Received: 3 March 2023; **Revised:** 28 March 2023; **Accepted:** 20 July 2023

Abstract: This paper deals with the effects of magnetic fields on unsteady Casson blood fluid flow in a stenosis artery. The effects of thermo-diffusion, thermal radiation, metabolic heat sources, and heat absorption are also considered. The flow is confined by the oscillating pressure gradient. The governing equations are remodeled into a system of PDEs in cylindrical form, which is then converted to dimensionless form using the similarity transformation. A definition of the Caputo-Fabrizio fractional order derivative is applied to the governing dimensionless form. The Laplace transform and the finite Hankel transform are used to obtain the analytic results. From the graphical results, it is illustrated that the external magnet reduced the rate of blood flow. It is also deduced that radiation tends to improve the rate of heat transfer, whereas the thermo-diffusion parameter tends to reduce the mass transfer process.

Keywords: stenosed artery, magnetic field, thermal diffusion, Casson fluid, magnetic particles, thermal radiation, fractional derivative

Nomenclature

$2\pi_c$	A critical value of this model
α	Fractional parameter
A_0	Systolic pressure gradient
A_1	Diastolic pressure gradient
\bar{B}	Magnetic field
$\beta = \frac{\mu_B \sqrt{2\pi_c} \mu}{\tau_r}$	Casson fluid's material parameter
D	Differential operator
\bar{d}	Stenosis location
F	Inclination angle parameter
f_p	Frequency of the pulse

G	Particle mass parameter
γ	Casson fluid parameter
H_a	Non-dimensional Hartman number
K	Stokes constant
K_c	Chemical reaction parameter
$\frac{KN}{\rho}(v-u)$	Force of relative motion between blood and magnetic particles
λ	Relaxation time
L_0	Stenosis length
m	The average mass of magnetic particles
μ_B	Plastic dynamic viscosity
N	Magnetic particles number
Nr	Thermal radiation parameter
ω	Pulsatile frequency
$\omega = 2\pi f_p$	Angular frequency
P	Oscillating pressure gradient
P_e	Peclet number
\varnothing	Phase angle
Q_m	Metabolic heat source
r	Radial coordinator
ρ	Fluid density
$R = \frac{KN\lambda}{\rho}$	Non-dimensional particle concentration parameter
R_0	Regular artery radius
$R_e = \frac{R_z^2}{\lambda\nu}$	Reynolds number
S	Laplace transform parameter
S_c	Schmidt number
σ	Electrical conductivity
S_r	Soret parameter
τ_r	Yield stress
θ_m	Metabolic heat absorption
$u(r, t)$	The velocity of the fluid
$v(r, t)$	The velocity of the particle
ν	Kinematic viscosity

1. Introduction

The new subfield of fluid mechanics is called bio-magnetic fluid dynamics (BFD), and it focuses on the performance of fluids subjected to magnetic fields [1]. BFD has a significant impact on many areas of medical engineering, bio-medical engineering, blood clotting, and the destruction of cancerous tumors [2, 3]. Haik et al. [4] introduced the BFD model to examine the motion of bio-magnetic fluid blood. Magnetohydrodynamics (MHD) studies an electrically conducting fluid in a magnetic field and is used in industry and engineering [5]. Primarily explored electromagnetic flow with application in measuring blood flow by Kolin [6], and MHD device usage to treat cardiovascular diseases by slowing blood flow was further explored by Korchevskii and Marochnick [7]. Several

scholars have looked at blood flow as a non-Newtonian fluid that behaves like magnetohydrodynamics; this concept is discussed in ref. [8, 9]. Habu et al. [10] concluded that an external magnetic field can control blood flow. Shit and Majee [11] observed that body vibration can impact the axial wave profile, temperature, and flow rate. The oscillatory flow of viscous fluid in a thin-walled tube exposed to elasticity and a magnetic field has been researched to treat localized diseases like cancer. Tzirtzilakis [12] developed a mathematical model that could explain the importance of BFD through an external magnetic field. In the occurrence of a magnetic field, Vincent et al. [13] investigated the velocity profile of turbulent blood flow in inclined arteries. Tripathy and Sharma [14] looked at how different viscosities affected MHD-inclined arterial blood flow when chemical reactions were involved. Unsteady MHD blood flow across a parallel channel plate was mathematically analyzed by Eldesoky [15]. His research found that when the heat source increases, the axial velocity and temperature rise, but the normal velocity and Prandtl number fall. Heat transport and blood flow in the circulatory system have been investigated for a long time for their potential role in the control of body temperature. A model of BFD with heat transfer in arteries was suggested by Chao [2].

Examining the fractional-order derivatives of the effects of a magnetic field, thermal diffusion, and body acceleration on blood flow is unique. In 1695, Leibniz first planned the idea of fractional calculus, and in 1832, Liouville expanded on this idea. Fractional derivatives have been effectively employed in many fields, including fluid mechanics, biology, mathematics, economics, etc. As per Caputo fractional derivatives, Laplace, and finite Hankel transforms, an external magnetic field reduced the motion and heat transfer processes [16]. The effect of magnetic fields on Casson fluid was investigated by Ali et al. [17] in their research on magnetic particles and blood flow. Recently, many researchers discussed the fractional time derivative model for blood flow problems [18-21].

The Soret effect refers to the thermo-diffusion phenomenon that occurs when there is a temperature gradient. The study of heat and mass transfer phenomena in porous mediums is studied theoretically and experimentally to build blood flow devices in biomedical engineering and technology. Ellahi et al. [22] examined nanoparticle-enhanced peristaltic pulsatile blood flow with a chemical reaction. Hayat et al. [23] studied the thermo-diffusion effect on peristaltic flow to calculate blood concentration. Khan et al. [24] studied the cross-diffusion effect on second-grade fluid flow. The cross-diffusion effects on the MHD flow of ferromagnetic fluid were theoretically investigated by Vafai et al. [25].

In this research, the fractional time derivative simulation of MHD Casson blood is discussed with stenosed arteries. The analytical expression of blood velocity, magnetic particle velocity, temperature profiles and concentration profiles are obtained using Laplace and Finite Hankel transformation. The mathematical analysis of said problems is useful for improving human health. From the results, it is concluded that the magnetic particle tends to reduce the blood viscosity, which is useful for controlling the blood flow velocity. Due to this result, we can improve the health condition of cardiovascular disease patients. Hence, these works can be helpful in solving many cardiovascular disease problems that disturb the regular rate of blood flow. This solution can be used to treat hypotension by bringing the patient's blood pressure up to a healthy level. Magnetic fields at different angles effectively reduce strokes, swellings, and pains.

2. Mathematical formulation

The focus of the current research is on unsteady fluid flow in an angled stenosed artery, which is outlined in Figure 1 and z -axis indicates axial direction, while the r -axis indicates radial direction. The model was developed using the incompressible Casson blood fluid that is accelerated through fluctuating pressure.

Figure 1 displays a graphic of the magnetic field that is delivered to the body to increase blood flow, with the generated magnetic field considered to be minimal. At time zero, both the blood and the magnetic particles were at rest. Blood flow and heat transfer are modeled using the Navier-Stokes and energy equations, while the magnetic field is described by Maxwell's relations and particle motion is governed by Newton's second law.

$$\frac{\partial T}{\partial t} = \frac{K_1}{\rho C_p} \left(\frac{\partial^2 T}{\partial r^2} + \frac{1}{r} \frac{\partial T}{\partial r} \right) - \frac{1}{\rho C_p} \frac{\partial q}{\partial r} + \frac{Q_m + \theta_m}{\rho C_p} \quad (5)$$

The concentration equation in the cylindrical coordinate can be written as

$$\frac{\partial C}{\partial t} = D_m \left(\frac{\partial^2 C}{\partial r^2} + \frac{1}{r} \frac{\partial C}{\partial r} \right) + \frac{D_m K_T}{T_\infty} \left(\frac{\partial^2 T}{\partial r^2} + \frac{1}{r} \frac{\partial T}{\partial r} \right) - K_2 (C - C_\infty). \quad (6)$$

The approximated heat flux, which appears in equations (5), is considered

$$-\frac{\partial q}{\partial r} = 4\alpha_1^2 (T - T_\infty), \text{ where } \alpha_1^2 = \int_0^\infty \beta_1 \chi \frac{\partial B}{\partial T}. \quad (7)$$

Where $\beta_1, \chi, \frac{\partial B}{\partial T}$ denote the radiative absorption coefficient, Planck's constant, and the frequency, respectively.

To consider the time-fractional model, equations (3) to (6) will be multiplied by $\lambda = \sqrt{\frac{R_0 \rho}{A_0}}$ to yield a term. So, equations (3) to (6) can be written in fractional derivative form as

$$\lambda^\alpha D_t^\alpha u = -\frac{\lambda}{p} (A_0 + A_1 \cos(\omega t)) + \lambda v \left(1 + \frac{1}{\beta} \right) \left(\frac{\partial^2 u}{\partial r^2} + \frac{1}{r} \frac{\partial u}{\partial r} \right) + \frac{KN\lambda}{\rho} (v - u) - \frac{\sigma \beta_0^2 \sin \theta \lambda}{\rho} v + g \lambda \sin \varnothing \quad (8)$$

$$\lambda^\alpha D_t^\alpha v = \frac{K\lambda}{m} (u - v) \quad (9)$$

$$\lambda^\alpha D_t^\alpha T = \frac{K\lambda}{\rho C_p} \left(\frac{\partial^2 T}{\partial r^2} + \frac{1}{r} \frac{\partial T}{\partial r} \right) - \frac{1}{\rho C_p} \frac{\partial q}{\partial r} + \frac{Q_m + \theta_m}{\rho C_p} \quad (10)$$

$$\lambda^\alpha D_t^\alpha \phi = D_m \lambda \left(\frac{\partial^2 C}{\partial r^2} + \frac{1}{r} \frac{\partial C}{\partial r} \right) + \frac{\lambda D_m K_T}{T_\infty} \left(\frac{\partial^2 T}{\partial r^2} + \frac{1}{r} \frac{\partial T}{\partial r} \right) - K_2 (C - C_\infty) \quad (11)$$

where Caputo-Fabrizio operator is

$${}^{CF}D_t^\alpha u(r, t) = \frac{1}{1-\alpha} \int_0^t \exp\left(-\frac{\alpha(t-\tau)}{1-\alpha}\right) \frac{\partial u(r, \tau)}{\partial \tau} d\tau.$$

The Laplace transform of Caputo-Fabrizio operator can be express as

$$L\{{}^{CF}D_t^\alpha u(r, t)\} = \frac{sL\{u(r, t) - u(r, 0)\}}{(1-\alpha)s + \alpha} \quad (13)$$

with $\alpha(0 < \alpha < 1)$ being the fractional order parameter.

The initial and boundary condition with stenosed artery of radius R_2 are

$$u(r, 0) = v(r, 0) = T(r, 0) = 0 \text{ at } r \in [0, R_z]$$

$$u(r, t) - v(r, t) = T(r, t) = 0 \text{ at } r = R_z \quad (14)$$

The non-dimensional parameters can be expressed as

$$r^* = \frac{r}{R_0}, t^* = \frac{t}{\lambda}, u^* = \frac{u}{u_0}, A_0^* = \frac{\lambda A_0}{\rho u_0}, A_1^* = \frac{\lambda A_1}{\rho u_0}, \omega^* = \lambda \omega, g^* = \frac{g}{\frac{u_0^2}{R_0}}$$

$$g^* = \frac{g}{\frac{u_0^2}{R_0}}, Nr = \frac{\alpha_1^2 R_0^2}{K}, \theta = \frac{T - T_\omega}{T_\omega - T_\infty}, p_r = \frac{\mu C_p}{k}, R_e = \frac{R_0 u_0}{\nu}, P_e = R_e \cdot P_r, S_c = \frac{\nu}{Dm},$$

$$S_r = \frac{D_m K_T (T_\omega - T_\infty)}{\nu T_\infty (C_\omega - C_\infty)}, \varnothing = \frac{C - C_\infty}{C_\omega - C_\infty}, Q_m = \frac{R_0 \overline{Q_m}}{u_0 \rho c_p (T_\omega - T_\infty)}, \theta_m = \frac{R_0 \overline{\theta_m}}{u_0 \rho c_p (T_\omega - T_\infty)}$$

The dimensionless form of equations (8) to (11) can be written as

$$D_t^\alpha u = \beta_1 \left[\frac{\partial^2 u}{\partial r^2} + \frac{1}{r} \frac{\partial u}{\partial r} \right] + R(v - u) - Ha^2 u + \frac{\sin}{F} + A_0 + A_1 \cos(\omega t) \quad (15)$$

$$GD_t^\alpha v = u - v \quad (16)$$

$$P_e D_t^\alpha \theta = \left(\frac{\partial^2 \theta}{\partial r^2} + \frac{1}{r} \frac{\partial \theta}{\partial r} \right) + Nr \theta + P_e (Q_m + \theta_m) \quad (17)$$

$$R_e S_c \phi = \left(\frac{\partial^2 \phi}{\partial r^2} + \frac{1}{r} \frac{\partial \phi}{\partial r} \right) + S_r S_c \left(\frac{\partial^2 \theta}{\partial r^2} + \frac{1}{r} \frac{\partial \theta}{\partial r} \right) - S_c K_c R_e^2 \phi \quad (18)$$

with boundary conditions

$$u\left(\frac{r}{R_z}, 0\right) = 0, v\left(\frac{r}{R_z}, 0\right) = 0, \theta\left(\frac{r}{R_z}, t\right) = 0 \text{ \& } \varnothing\left(\frac{r}{R_z}, 0\right) = 0 \text{ at } \frac{r}{R_z} \in [0, 1]$$

$$u\left(\frac{r}{R_z}, t\right) = 0, v\left(\frac{r}{R_z}, t\right) = 0, \theta\left(\frac{r}{R_z}, t\right) = 0 \text{ \& } \varnothing\left(\frac{r}{R_z}, t\right) \text{ at } \frac{r}{R_z} = 1. \quad (19)$$

3. Solution of the problem

Now, the Laplace transform technique is applied in equations (15) to (18), we obtain

$$\frac{S\bar{u}(r,s)}{S+\alpha(1-s)} = \frac{A_0}{S} + \frac{A_1S}{s^2+\omega^2} + \beta_1 \left(\frac{\partial^2 \bar{u}(r,s)}{\partial r^2} + \frac{1}{r} \frac{\partial \bar{u}(r,s)}{\partial r} \right) + R\bar{v} - (R+Ha^2)\bar{u}(r,s) + \frac{\sin \phi}{SF}, \quad (20)$$

$$G \frac{S\bar{v}(r,s)}{S+\alpha(1-s)} = \bar{u}(r,s) - \bar{v}(r,s), \quad (21)$$

$$P_e \frac{S\bar{\theta}(r,s)}{S+\alpha(1-s)} = \left[\frac{\partial^2 \bar{\theta}(r,s)}{\partial r^2} + \frac{1}{r} \frac{\partial \bar{\theta}(r,s)}{\partial r} \right] + Nr\bar{\theta}(r,s) + P_e \frac{Q_m + \theta_m}{S}, \quad (22)$$

$$R_e S_c \frac{S\bar{\vartheta}(r,s)}{S+\alpha(1-s)} = \left(\frac{\partial^2 \bar{\vartheta}(r,s)}{\partial r^2} + \frac{1}{r} \frac{\partial \bar{\vartheta}(r,s)}{\partial r} \right) + S_r S_c \left(\frac{\partial^2 \bar{\theta}(r,s)}{\partial r^2} + \frac{1}{r} \frac{\partial \bar{\theta}(r,s)}{\partial r} \right) - S_c K_c R_e^2 \bar{\vartheta}(r,s). \quad (23)$$

With boundary condition $\bar{u}(1,s) = \bar{v}(1,s) = \bar{\theta}(1,s) = 0$ from equation (21),

$$\bar{v}(r,s) = \frac{\alpha(1-\alpha) + S}{\alpha(1-s) + S + GS} \bar{u}(r,s). \quad (24)$$

Inputs equation (24) into equation (20),

$$\left[\frac{s}{S+\alpha(1-s)} - R \left(\frac{S+\alpha(1-\alpha)}{GS+s+\alpha(1-s)} \right) + R + Ha^2 \right] \bar{u}(r,s) = \frac{A_0}{S} + \frac{A_1S}{s^2+\omega^2} + \beta_1 \left(\frac{\partial^2 \bar{u}}{\partial r^2} + \frac{r}{r} \frac{\partial \bar{u}}{\partial r} \right) + \frac{\sin \phi}{SF} \quad (25)$$

Applying the finite Hankel transformation of order zero in equations (25) and (22) with the boundary condition (19), the following equation can be obtained:

$$\left[\frac{s}{\alpha(1-s) + S} - \left(\frac{S+\alpha(1-\alpha)}{GS+S+\alpha(1-s)} \right) R + R + Ha^2 \right] \bar{u}_H(r_n,s) \left[\frac{\sin \phi}{SF} + \frac{A_1S}{s^2+\omega^2} + \frac{A_0}{S} \right] \frac{J_1(r_n)}{r_n} - r_n \beta_1 \bar{u}_H(r_n,s) \quad (26)$$

$$P_e \frac{S\bar{\theta}_H(r_n,s)}{S+\alpha(1-s)} = -r_n \bar{\theta}_H(r_n,s) - Nr \bar{\theta}_H(r_n,s) + \frac{Q_m + \theta_m}{S} \cdot \frac{J_1(r_n)}{r_n} \quad (27)$$

$$R_e S_c \frac{S\bar{\vartheta}_H(r,s)}{S+\alpha(1-s)} = -r_n \bar{\vartheta}_H(r_n,s) + S_r S_c (-r_n) \bar{\theta}_H(r_n,s) - S_c K_c R_e^2 \bar{\vartheta}_H(r_n,s) \quad (28)$$

where $\bar{u}_H(r_n,s) = \int_0^1 r \bar{u}(r,s) J_0(r_n,r) dr$ represents the finite Hankel transformation of the velocity and temperature function.

Here, $J_0(x) = 0$, J_0 is first kind zero order Bessel's function, and $r_n, n = 1, 2, 3, \dots$ are the positive roots of equation.

Reform of equations (26) to (28), we get

$$\overline{u_H}(r_n, s) = \frac{S^2 B_5 + SB_6 + \alpha^2}{S^2 B_2 + SB_3 + B_4} \left[\frac{1}{s} \left(A_0 + \frac{\sin \phi}{F} + \frac{A_1 S}{s^2 + \omega^2} \right) \right] \frac{J_1(r_n)}{r_n} \quad (29)$$

$$\therefore \overline{u_H}(r_n, s) = \left[\frac{B_9}{S - B_7} + \frac{B_{10}}{S - B_8} \right] \left[\frac{1}{s} \left(A_0 + \frac{\sin \phi}{F} + \frac{A_1 S}{s^2 + \omega^2} \right) \right] \frac{J_1(r_n)}{r_n} \quad (30)$$

$$\therefore \overline{u_H}(r_n, s) = \left(A_0 + \frac{\sin \phi}{F} \right) \left[B_9 \frac{S^{-1}}{S - B_7} + B_{10} \frac{S^{-1}}{S - B_8} \right] \frac{J_1(r_n)}{r_n} + \frac{A_1 S}{s^2 + \omega^2} \left[\frac{1}{S - B_7} B_9 + \frac{1}{S - B_8} B_{10} \right] \frac{J_1(r_n)}{r_n} \quad (31)$$

Similarly, when we process the energy equation (27), we get

$$\overline{\theta_H}(r_n, s) = \frac{Pe(Q_m + \theta_m)}{S \left[r_n + Pe \frac{S}{S + \alpha(1-s)} + Nr \right]} \cdot \frac{J_1(r_n)}{r_n} \quad (32)$$

Now, rearrange the equation (32)

$$\overline{\theta_H}(r_n, s) = \left[\frac{1}{S + B_{15}} B_{13} + \frac{1}{S - B_{15}} B_{14} \right] \frac{J_1(r_n)}{r_n} \quad (33)$$

Similarly, when we process the concentration equation (28), we get

$$\frac{R_e S_c S \overline{\varnothing_H}(r, s)}{S + \alpha(1-s)} = \left[\frac{S_r S_c (-r_n) P_e (Q_m + \theta_m)}{S \left[r_n + Pe \frac{S}{S + \alpha(1-s)} + Nr \right]} \right] \cdot \frac{J_1(r_n)}{r_n} - S_c K_c R_e^2 \overline{\varnothing_H}(r_n, s) - r_n \overline{\varnothing_H}(r_n, s) \quad (34)$$

$$\left[\frac{R_e S_c S}{S + \alpha(1-s)} + S_c K_c R_e^2 + r_n \right] \overline{\varnothing_H}(r, s) = \left[\frac{-r_n S_r S_c P_e (Q_m + \theta_m)}{S \left[r_n + Pe \frac{S}{S + \alpha(1-s)} + Nr \right]} \right] \cdot \frac{J_1(r_n)}{r_n} \quad (35)$$

$$\overline{\varnothing_H}(r, s) = - \frac{S_r S_c r_n P_e (Q_m + \theta_m)}{\left(S \left[r_n + Nr + Pe \frac{S}{S + \alpha(1-s)} \right] \right) \left[\frac{R_e S_c S}{S + \alpha(1-s)} + r_n + S_c K_c R_e^2 \right]} \cdot \frac{J_1(r_n)}{r_n} \quad (36)$$

Now, rearrange the equation (36)

$$\overline{\varnothing_H}(r, s) = \frac{B_{16}}{\left(S \left[B_{17} + Pe \frac{S}{S + \alpha(1-s)} \right] \right) \left[\frac{B_{19} S}{S + \alpha(1-s)} + r_n + B_{18} \right]} \cdot \frac{J_1(r_n)}{r_n} \quad (37)$$

$$\overline{\vartheta}_H(r,s) = \frac{B_{16}(S + \alpha(1-S))^2}{S(B_{17}S + B_{17}\alpha - B_{17}\alpha S + P_e S)(B_{19}S + B_{18}\alpha + B_{18}S - B_{18}\alpha S)} \cdot \frac{J_1(r_n)}{r_n} \quad (38)$$

$$\overline{\vartheta}_H(r,s) = \frac{B_{16}(S + \alpha(1-S))^2}{S((B_{17} - B_{17}\alpha + P_e)S + B_{17}\alpha)((B_{19} + B_{18} - B_{18}\alpha)S + B_{18}\alpha)} \cdot \frac{J_1(r_n)}{r_n} \quad (39)$$

$$\overline{\vartheta}_H(r,s) = \frac{B_{16}(S + \alpha(1-S))^2}{S(B_{20}S + B_{22})(B_{21}S + B_{23})} \cdot \frac{J_1(r_n)}{r_n} \quad (40)$$

$$\overline{\vartheta}_H(r,s) = \frac{B_{16}}{B_{20} \cdot B_{21}} \frac{(a^2 + 2\alpha(1-\alpha)S + (1-\alpha)^2 S^2)}{S\left(S + \frac{B_{22}}{B_{20}}\right)\left(S + \frac{B_{23}}{B_{21}}\right)} \cdot \frac{J_1(r_n)}{r_n} \quad (41)$$

$$\overline{\vartheta}_H(r,s) = \frac{B_{16}}{B_{20} \cdot B_{21}} \frac{(a^2 + 2\alpha(1-\alpha)S + (1-\alpha)^2 S^2)}{S\left(S + \frac{B_{22}}{B_{20}}\right)\left(S + \frac{B_{23}}{B_{21}}\right)} \cdot \frac{J_1(r_n)}{r_n} \quad (42)$$

$$\overline{\vartheta}_H(r,s) = \frac{B_{24}(\alpha^2 + B_{25}S + B_{26}S^2)}{S(S + B_{27})(S + B_{28})} \cdot \frac{J_1(r_n)}{r_n} \quad (43)$$

$$\overline{\vartheta}_H(r,s) = \left(\frac{B_{29}}{S} + \frac{B_{30}}{S + B_{27}} + \frac{B_{29}}{S + B_{28}} \right) \cdot \frac{J_1(r_n)}{r_n} \quad (44)$$

The inverse Laplace transform of $\overline{\vartheta}_H(m,s)$ find using the Hartley's function and Robotnov function,

$$LT^{-1} \left[\frac{q}{S^\omega + y} \right] = F_\omega(-y, t) = \sum_{n=0}^{\infty} \frac{(-y)^n t^{(n+1)\omega-1}}{\Gamma(n+1)\omega}; \omega > 0 \quad (45)$$

$$LT^{-1} \left[\frac{S^z}{S^w + y} \right] = R_{w,z}(-y, t) = \sum_{n=0}^{\infty} \frac{(-y)^n t^{(n+1)w-1-z}}{\Gamma((n+1)w-z)}; \text{Re}(w-z) > 0 \quad (46)$$

Now, applying the inverse Laplace transform of equations (31), (33), and (44) are

$$\therefore \overline{u}_H(r_n, t) = \frac{J_1(r_n)}{r_n} \left[\left(e^{B_7 t} - 1 \right) \left(\frac{A_0}{B_7} B_9 + \frac{B_9 \sin \phi}{B_7 F} \right) + \left(e^{B_8 t} - 1 \right) \left(\frac{A_0}{B_8} B_{10} + \frac{B_{10} \sin \phi}{B_8 F} \right) + \right. \\ \left. A_1 B_9 e^{B_7 t} * \cos(\omega t) + A_1 B_{10} e^{B_8 t} * \cos(\omega t) \right] \quad (47)$$

$$\therefore \overline{\theta}_H(r_n, t) = \frac{J_1(r_n)}{r_n} \left[B_{13}e^{-B_{15}t} + \frac{B_{14}}{B_{15}}(1 - e^{-B_{15}t}) \right] \quad (48)$$

$$= \frac{J_1(r_n)}{r_n} [B_{13}F_1(-B_{15}, t) + B_{14}R_{i-1}(-B_{15}, t)] \quad (49)$$

$$\therefore \overline{\varnothing}_H(r_n, t) = \frac{J_1(r_n)}{r_n} [B_{29} + B_{30}e^{-B_{27}t} + B_{31}e^{-B_{31}t}] \quad (50)$$

Fluid velocity and temperature are obtained by taking the inverse Hankel transformation of equations (47), (48), and (50)

$$u(r, t) = 2 \sum_{n=1}^{\infty} \frac{J_0\left(\frac{r}{r_z} r_n\right)}{r_n J_1^2(r_n)} \times u_H(r_n, t) \quad (51)$$

$$u(r, t) = 2 \sum_{n=1}^{\infty} \frac{J_0\left(\frac{r}{r_z} r_n\right)}{r_n J_1^2(r_n)} \left[\left(e^{B_7 t} - 1 \right) \left(\frac{A_0}{B_7} B_9 + \frac{B_9 \sin \phi}{B_7 F} \right) + \left(e^{B_8 t} - 1 \right) \left(\frac{A_0}{B_8} B_{10} + \frac{B_{10} \sin \phi}{B_8 F} \right) + \right. \\ \left. A_1 B_9 e^{B_7 t} * \cos(\omega t) + A_1 B_{10} e^{B_8 t} * \cos(\omega t) \right] \quad (52)$$

$$\theta(r, t) = 2 \sum_{n=1}^{\infty} \frac{J_0\left(\frac{r}{r_z} r_n\right)}{r_n J_1^2(r_n)} \times \theta_H(r_n, t) \quad (53)$$

$$\theta(r, t) = 2 \sum_{n=1}^{\infty} \frac{J_0\left(\frac{r}{r_z} r_n\right)}{r_n J_1^2(r_n)} \times \left[B_{13}e^{-B_{15}t} + \frac{B_{14}}{B_{15}}(1 - e^{-B_{15}t}) \right] \quad (54)$$

$$\varnothing(r, t) = 2 \sum_{n=1}^{\infty} \frac{J_0\left(\frac{r}{r_z} r_n\right)}{r_n J_1^2(r_n)} \times \varnothing_H(r_n, t) \quad (55)$$

$$\varnothing(r, t) = 2 \sum_{n=1}^{\infty} \frac{J_0\left(\frac{r}{r_z} r_n\right)}{r_n J_1^2(r_n)} \times [B_{29} + B_{30}e^{-B_{27}t} + B_{31}e^{-B_{31}t}] \quad (56)$$

The velocity of a magnetic particle can be expressed from equation (24)

$$\bar{v}(r, s) = \frac{S + \alpha - \alpha s}{GS + S + \alpha(1 - s)} \bar{u}(r, s) \quad (57)$$

$$v(r, t) = B_{33}(1 - B_{32})[u(r, t) * e^{B_{12}t}], 0 < \alpha < 1 \quad (58)$$

4. Numerical results and analysis

By analyzing the effects of various physical parameters on the velocities of blood, magnetic particle velocity, temperature, and concentration profiles, numerical results are obtained and presented in Figures 2 to 16. For the numerical calculations, the following parameters are fixed: $A_0 = 0.5$, $A_1 = 0.1$, $\omega = \frac{\pi}{4}$, $R_e = 2$, $G = 2$, $H_a = 1$, and $R = 0.5$. In this model, the values of fractional order derivative are considered as $\alpha = 0.2, 0.6$, and 1 .

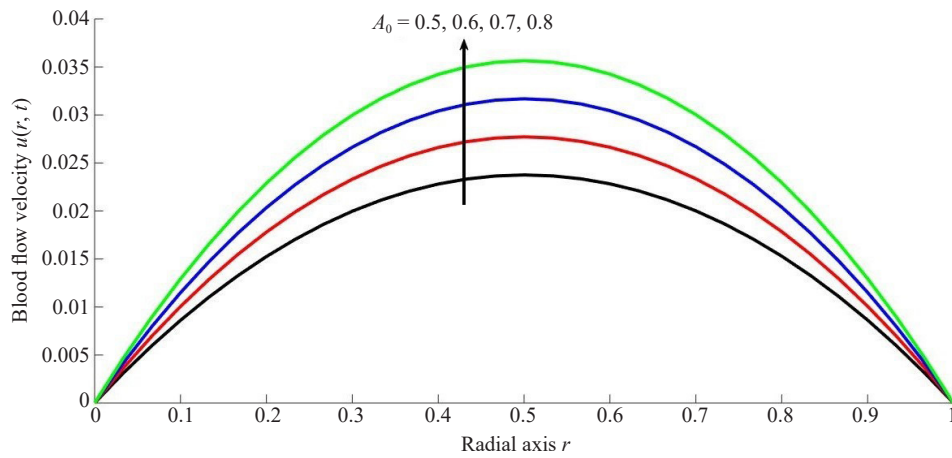


Figure 2. $u(r, t)$ for A_0

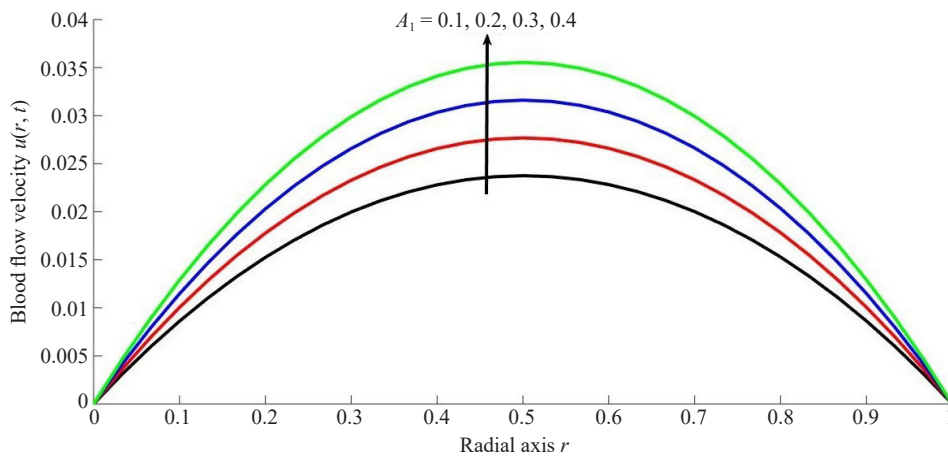


Figure 3. $u(r, t)$ for A_1

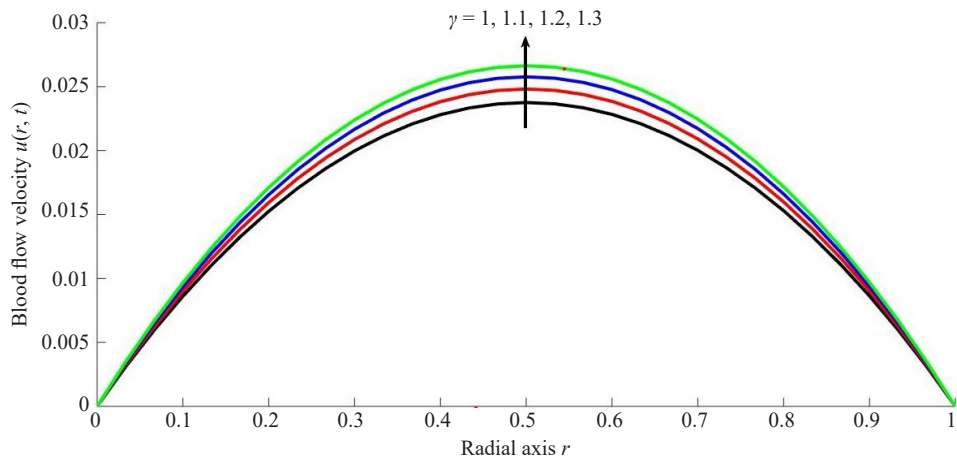


Figure 4. $u(r, t)$ for γ

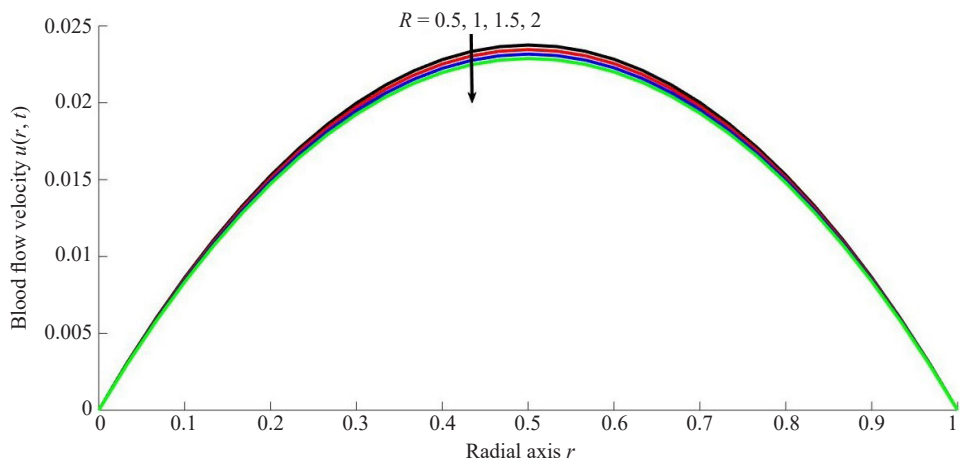


Figure 5. $u(r, t)$ for R

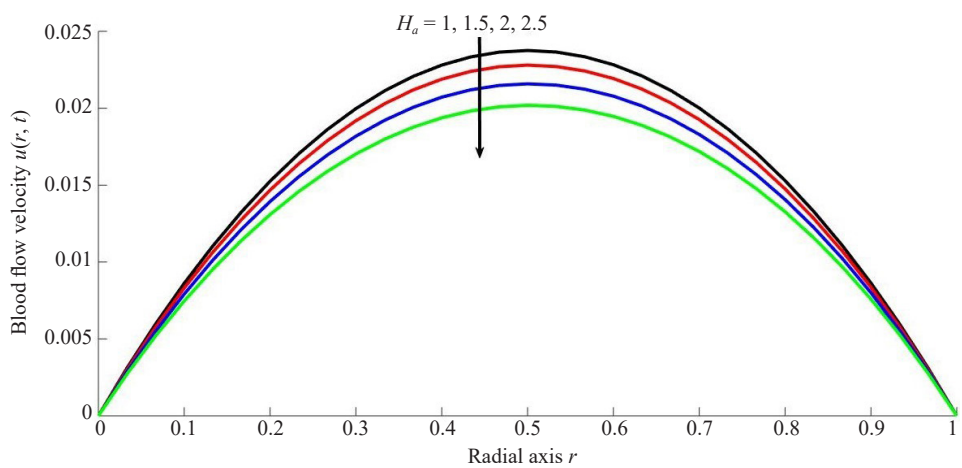


Figure 6. $u(r, t)$ for H_a

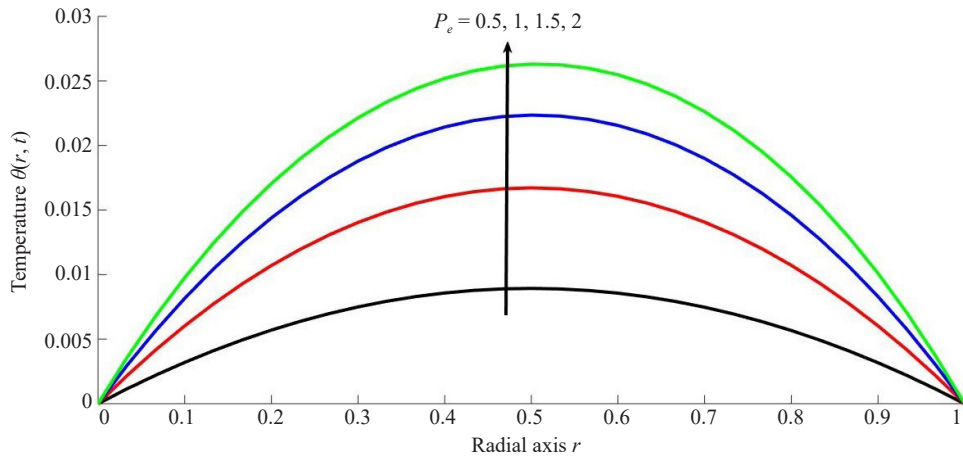


Figure 7. $\theta(r, t)$ for P_e

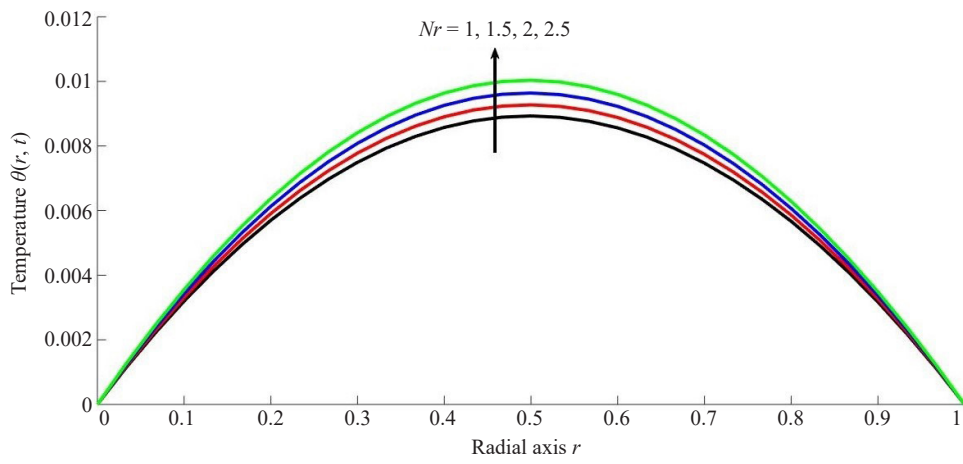


Figure 8. $\theta(r, t)$ for Nr

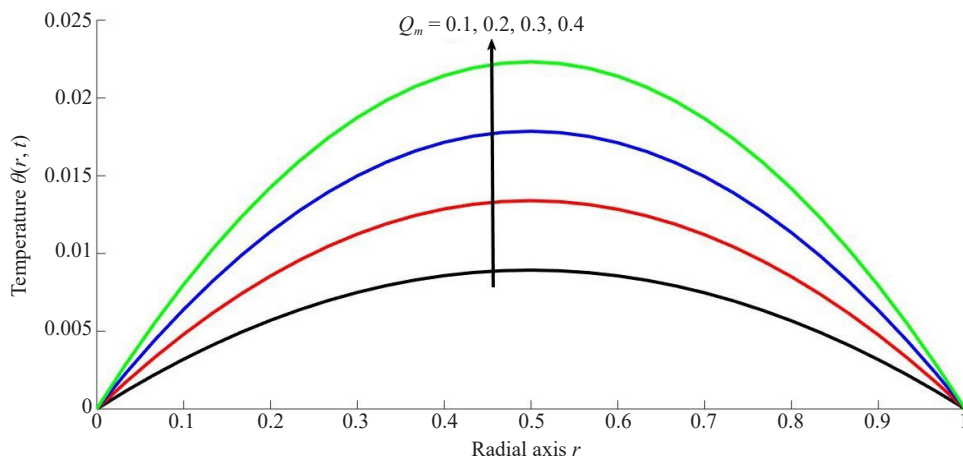


Figure 9. $\theta(r, t)$ for Q_m

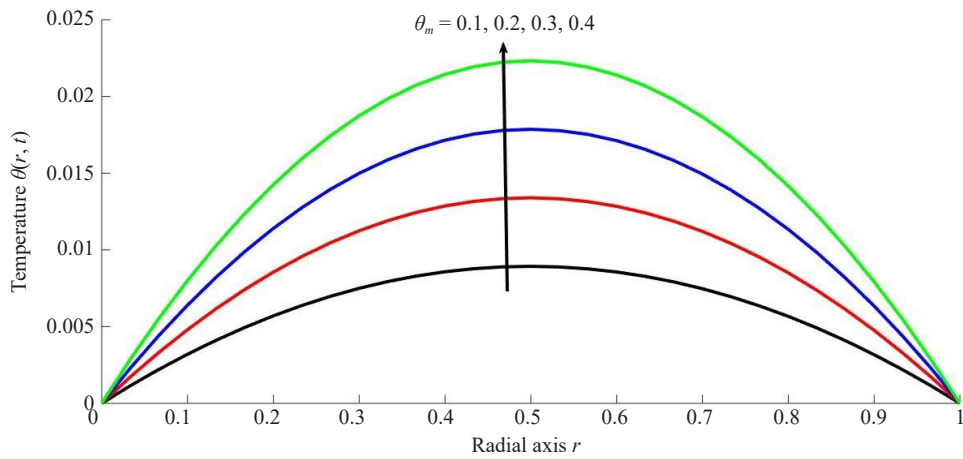


Figure 10. $\theta(r, t)$ for θ_m

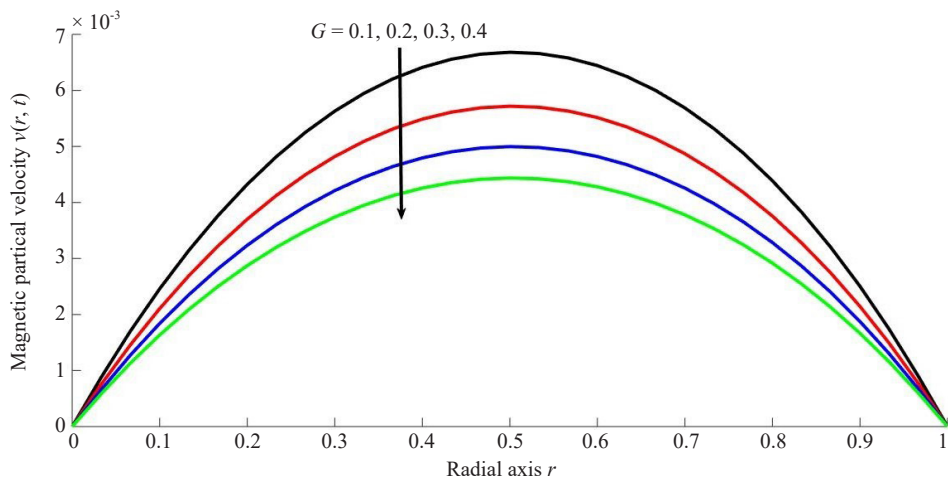


Figure 11. $v(r, t)$ for G

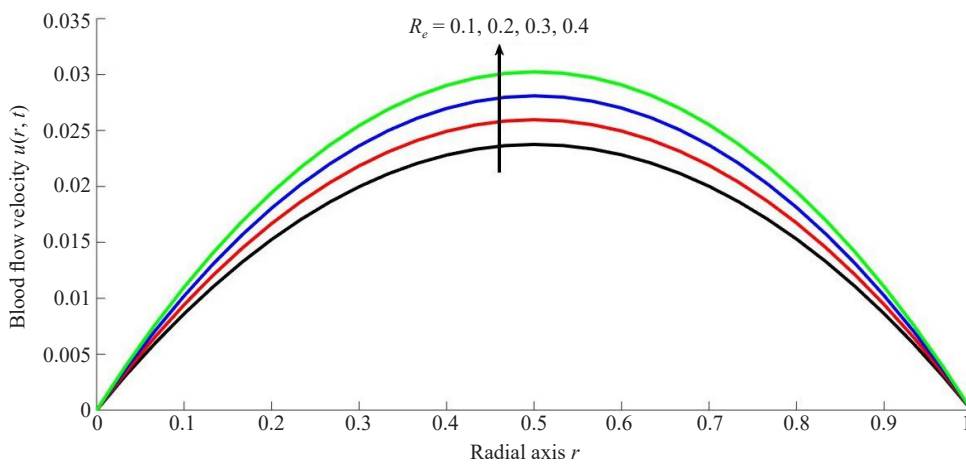


Figure 12. $u(r, t)$ for R_e

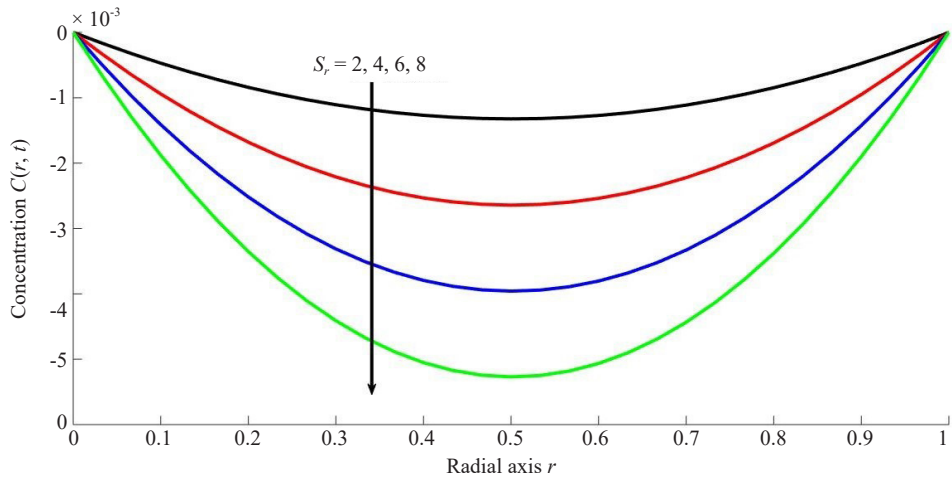


Figure 13. $C(r, t)$ for S_r

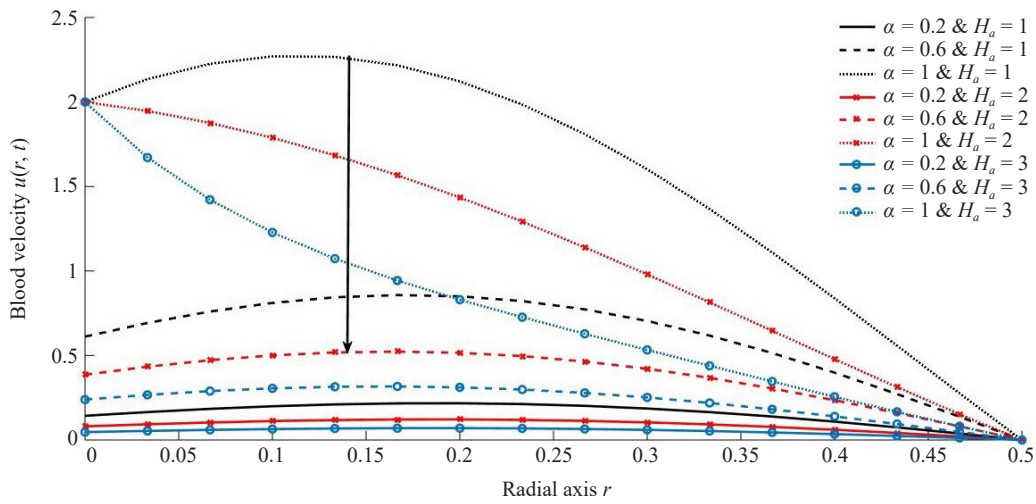


Figure 14. $u(r, t)$ for α and H_a

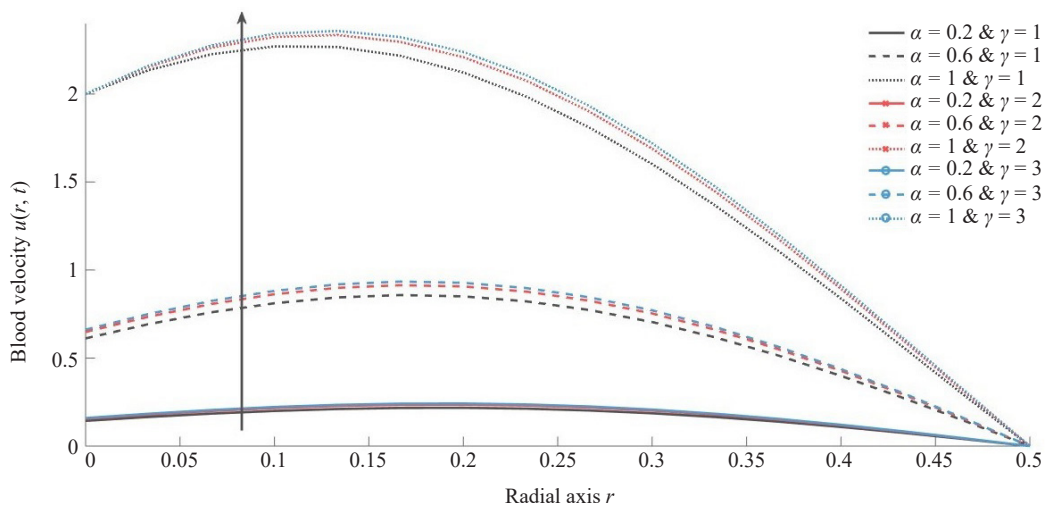


Figure 15. $u(r, t)$ for α and γ

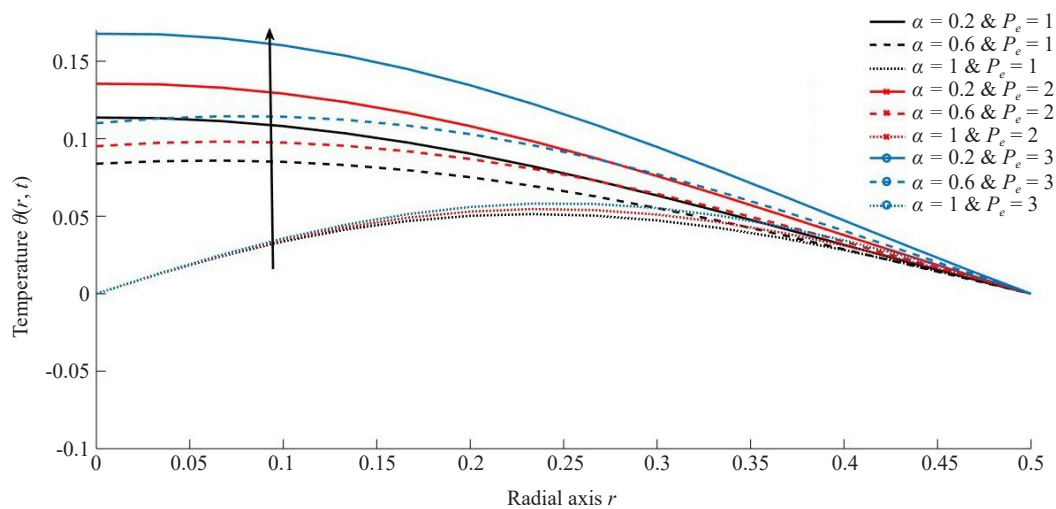


Figure 16. $\theta(r, t)$ for α and P_e

Figures 2 and 3 show the effects of the systolic pressure gradient and the diastolic pressure gradient on blood velocity. It is seen that the motion of the blood improves with increasing values of the parameters. Physically, when we increase the pressure gradient, fluid is accelerated, and due to this, the velocity of the blood flow is also increased. The non-Newtonian character of blood is reflected in the Casson parameter. Higher values of the Casson parameter are related to Newtonian nature. As can be seen in Figure 4, as the Casson parameter is raised, blood velocity increases. The increase in the Casson fluid parameter decreases the yield stress, and consequently, the boundary layer thickness decreases. Casson's behavior is more important in small arteries because of the possibility of red blood cell collection and distribution there owing to the rotation of the artery's axis. Figure 5 shows how the fluid motion is affected by the particle concentration R . It is seen that the blood velocity decreases with an increase in R .

The velocity profile has always been more strongly influenced by the magnetic field. To study the effect of Hartman number on blood flow, Figure 6 is plotted. The velocity of blood decreases with an increasing value of the Hartman number. During this time, the charged particles would be rotating due to the impact of a magnetic field. As a result of the magnetic orientation, red blood cells and magnetic particles would be maintained in suspension much longer. In addition to increasing blood viscosity, a greater concentration of magnetic particles will raise the axial flow rate. The magnetic fields can be used in the fluid flow model to increase the Lorentz force, which would reduce blood flow. Therapeutic applications and therapy procedures connected to atherosclerosis, fractured bones, controlled tissue damage, and cancer may benefit from a controllable magnetic field. Figure 7 shows the effect of the P_e on temperature profiles. It is illustrated that the P_e tends to improve the heat transfer process. The effects of thermal radiation parameters on temperature profiles are shown in Figure 8. Physically, when we increase the thermal radiation parameter, the blood becomes thin due to radiation, and hence the heat transfer process is improved. Figure 9 displays a variation in temperature at different metabolic heat sources. Increasing the metabolic heat source has a warming effect on temperature. In the absence of a metabolic heat source, blood vessel temperatures are lower. Temperatures in the system increased because of a metabolic heat source, while the wall temperature remained at zero to follow the boundary condition. The effect of increasing metabolic heat absorption on temperature is represented in Figure 10. The size of the particles is what determines the value of the parameter for the particle mass, known as G . According to Figure 11, the magnetic particle velocity tends to decrease as the mass parameter is increased. As shown in Figure 12, the velocity profiles vary with the Reynolds number. The Reynolds number is inversely proportional to the fluid's velocity. The fluid's velocity gradually increases as Reynold's number rises. Physically, lower viscosity (increased velocity) will increase. Figure 13 illustrates concentration profiles for various values of the thermos-diffusion parameter S_r . It is concluded that an increase in S_r decreases the concentration profile and the boundary layer thickness. The Soret effect, or thermo-diffusion, which is a driving factor for mass diffusion, may also be caused by a temperature gradient. Therefore, the Soret effect increases with an increasing temperature gradient.

Figures 14 to 16 show the effects of fractional order parameter α , magnetic parameter H_a , Casson parameter, and P_e on velocity and temperature profiles. All figures indicate the impact of the fractional order parameter on velocity and temperature profiles. It is also seen that velocity is increasing, whereas temperature decreases with increasing values of α . This result helps analyze the difference between a fractional-order derivative and an integer-order derivative. From Figures 14 to 16, the effects of H_a , H , and P_e are already discussed in previous figures.

5. Conclusion

The following are the key findings of the current study:

- It is notable that the axial velocity of blood flow can be controlled by applying an external magnetic field of the correct strength. Research into atherosclerosis treatment will benefit from this information.
- Heat transfer processes improve with increasing values of thermal radiation and P_e .
- The concentration level of the fluid rises with the fall due to the thermos-diffusion parameter. This result will be important to investigate during cancer hyperthermia treatment.
- The fractional order parameter α tends to improve the motion of the blood flow. Due to this, it is observed that blood velocity delays with the fractional-order model.
- Temperatures lower as the fractional parameters are increased, which implies that the heat transfer process is much faster for the fractional-order model.

Conflict of interest

There is no conflict of interest in this study.

References

- [1] Tzirtzilakis EE. A mathematical model for blood flow in magnetic field. *Physics of Fluids*. 2005; 17(7): 077103. Available from: <https://doi.org/10.1063/1.1978807>.
- [2] Chato JC. Condensation in smooth horizontal tubes. *Journal of Heat Transfer*. 1979; 102: 193-213.
- [3] Shaw S, Murthy PVS. Magnetic drug targeting in the permeable blood vessel-The effect of blood rheology. *Journal of Nanotechnology in Engineering and Medicine*. 2010; 1(2): 021001. Available from: <https://doi.org/10.1115/1.4001477>.
- [4] Pai V, Haik Y, Chen CJ. Bio magnetic fluid dynamics. *Engineering Mechanics*. 1996; 458-461.
- [5] Xenos MA, Tzirtzilakis EE. *Biomagnetic Fluid Flow in a Driven Cavity*. 2013. Available from: <http://campus.mst.edu/adsa> [Accessed 27 December 2024].
- [6] Leenov D, Kolin A. Theory of electromagnetophoresis. I. Magneto hydrodynamic forces experienced by spherical and symmetrically oriented cylindrical particles. *The Journal of Chemical Physics*. 1954; 22(4): 683-688. Available from: <https://doi.org/10.1063/1.1740149>.
- [7] Korchevskii EM, Marochnik LS. Magneto hydrodynamic version of movement of blood. *Biophysics*. 1965; 10(2): 411-413.
- [8] Misra JC, Shit GC. Flow of a biomagnetic visco-elastic fluid in a channel with stretching walls. *Journal of Applied Mechanics*. 2009; 76(6): 061006. Available from: <https://doi.org/10.1115/1.3130448>.
- [9] Abdulhameed M, Vieru D, Roslan R. Modeling electro-magneto-hydrodynamic thermo-fluidic transport of biofluids with new trend of fractional derivative without singular kernel. *Physica A: Statistical Mechanics and Its Applications*. 2017; 484: 233-252. Available from: <https://doi.org/10.1016/j.physa.2017.05.001>.
- [10] Habu PN, Attah F, Ibrahim H. Oscillatory motion of a viscous fluid in a thin-walled elastic tube with induced magnetic field: A proposed therapy for cancer and hypertension treatment. *Applied Mathematics*. 2015; 5(5): 97-100. Available from: <https://doi.org/10.5923/j.am.20150505.02>.
- [11] Shit GC, Majee S. Pulsatile flow of blood and heat transfer with variable viscosity under magnetic and vibration

- environment. *Journal of Magnetism and Magnetic Materials*. 2015; 388: 106-115. Available from: <https://doi.org/10.1016/j.jmmm.2015.04.026>.
- [12] Tzirakis K, Botti L, Vavourakis V, Papaharilaou Y. Numerical modeling of non-Newtonian biomagnetic fluid flow. *Computers & Fluids*. 2016; 126: 170-180. Available from: <https://doi.org/10.1016/j.compfluid.2015.11.016>.
- [13] Mwanthi V, Mwenda E, Gachoka KK. Velocity profiles of unsteady blood flow through an inclined circular tube with magnetic field. *Journal of Advances in Mathematics and Computer Science*. 2017; 24(6): 1-10. Available from: <https://doi.org/10.9734/jamcs/2017/36620>.
- [14] Tripathi B, Sharma BK. Effect of variable viscosity on MHD inclined arterial blood flow with chemical reaction. *International Journal of Applied Mechanics and Engineering*. 2018; 23(3): 767-785. Available from: <https://doi.org/10.2478/ijame-2018-0042>.
- [15] Eldesoky IM. Mathematical analysis of unsteady MHD blood flow through parallel plate channel with heat source. *World Journal of Mechanics*. 2012; 2(3): 131-137. Available from: <https://doi.org/10.4236/wjm.2012.23015>.
- [16] Shah NA, Vieru D, Fetecau C. Effects of the fractional order and magnetic field on the blood flow in cylindrical domains. *Journal of Magnetism and Magnetic Materials*. 2016; 409: 10-19. Available from: <https://doi.org/10.1016/j.jmmm.2016.02.013>.
- [17] Sheikh NA, Ali F, Khan I, Saqib M. A modern approach of Caputo-Fabrizio time-fractional derivative to MHD free convection flow of generalized second-grade fluid in a porous medium. *Neural Computing and Applications*. 2018; 30: 1865-1875. Available from: <https://doi.org/10.1007/s00521-016-2815-5>.
- [18] Oldham K, Spanier J. *The fractional calculus theory and applications of differentiation and integration to arbitrary order*. Elsevier; 1974.
- [19] Perdikaris P, Karniadakis GE. Fractional-order viscoelasticity in one-dimensional blood flow models. *Annals of Biomedical Engineering*. 2014; 42(5): 1012-1023. Available from: <https://doi.org/10.1007/s10439-014-0970-3>.
- [20] Abdullah M, Butt AR, Raza N, Alshomrani AS, Alzahrani AK. Analysis of blood flow with nanoparticles induced by uniform magnetic field through a circular cylinder with fractional Caputo derivatives. *Journal of Magnetism and Magnetic Materials*. 2018; 446: 28-36. Available from: <https://doi.org/10.1016/j.jmmm.2017.08.074>.
- [21] Maiti S, Shaw S, Shit GC. Caputo-Fabrizio fractional order model on MHD blood flow with heat and mass transfer through a porous vessel in the presence of thermal radiation. *Physica A: Statistical Mechanics and Its Applications*. 2020; 540: 123149. Available from: <https://doi.org/10.1016/j.physa.2019.123149>.
- [22] Elelami AF, Elgazery NS, Ellahi R. Blood flow of MHD non-Newtonian nanofluid with heat transfer and slip effects: Application of bacterial growth in heart valve. *International Journal of Numerical Methods for Heat & Fluid Flow*. 2020; 30(11): 4883-4908. Available from: <https://doi.org/10.1108/HFF-12-2019-0910>.
- [23] Hayat T, Aslam N, Khan MI, Khan MI, Alsaedi A. Physical significance of heat generation/absorption and Soret effects on peristalsis flow of pseudoplastic fluid in an inclined channel. *Journal of Molecular Liquids*. 2019; 275: 599-615. Available from: <https://doi.org/10.1016/j.molliq.2018.11.055>.
- [24] Khan AA, Naeem S, Ellahi R, Sait SM, Vafai K. Dufour and Soret effects on Darcy-Forchheimer flow of second-grade fluid with the variable magnetic field and thermal conductivity. *International Journal of Numerical Methods for Heat & Fluid Flow*. 2020; 30(9): 4331-4347.
- [25] Khaled ARA, Vafai K. The role of porous media in modeling flow and heat transfer in biological tissues. *International Journal of Heat and Mass Transfer*. 2003; 46(26): 4989-5003. Available from: [https://doi.org/10.1016/S0017-9310\(03\)00301-6](https://doi.org/10.1016/S0017-9310(03)00301-6).

Appendix:

$$B_1 = R + Ha^2 + B_1 r_n^2$$

$$B_2 = 1 + G - \alpha - R - R\alpha^2 + 2R\alpha + B_1 + B_1\alpha^2 - 2\alpha B_1 + GB_1 - G\alpha B_1$$

$$B_3 = \alpha + 2R\alpha^2 - 2R\alpha - 2B_1\alpha^2 + 2\alpha B_1 + G\alpha B_1$$

$$B_4 = B_1\alpha^2 - R\alpha^2, B_5 = 1 + \alpha^2 - 2\alpha + G + G\alpha, B_6 = -2\alpha^2 + 2\alpha + G\alpha$$

$$B_7 = \frac{-B_3 \pm \sqrt{B_3^2 - 4B_2B_4}}{2B_2}, B_8 = \frac{-B_3 \pm \sqrt{B_3^2 - 4B_2B_4}}{2B_2}, B_9 = \frac{B_7^2 B_5 + B_7 B_6 + \alpha^2}{B_7 - B_8},$$

$$B_{10} = \frac{B_8^2 B_5 + B_8 B_6 + \alpha^2}{B_8 - B_7}, B_{11} = (r_n + Nr)(1 - \alpha) + P_e, B_{12} = (r_n + Nr)\alpha$$

$$B_{13} = P_e \frac{(Q_m + \theta_m)(1 - \alpha)}{B_{11}}, B_{14} = P_e \frac{(Q_m + \theta_m)\alpha}{B_{11}}, B_{15} = \frac{B_{12}}{B_{11}},$$

$$B_{16} = -S_r S_c r_n P_e (Q_m + \theta_m), B_{17} = r_n + Nr, B_{18} = r_n + S_c K_c R_e^2,$$

$$B_{19} = R_e S_c, B_{20} = B_{17} - B_{17}\alpha + P_e, B_{21} = B_{19} + B_{18} - B_{18}\alpha, B_{22} = B_{17}\alpha$$

$$B_{23} = B_{18}\alpha, B_{24} = \frac{B_{16}}{B_{20} \cdot B_{21}}, B_{25} = 2\alpha(1 - \alpha), B_{26} = (1 - \alpha)^2, B_{27} = \frac{B_{22}}{B_{20}}$$

$$B_{28} = \frac{B_{23}}{B_{21}}, B_{29} = \frac{B_{24}(\alpha^2)}{B_{27} B_{28}}, B_{30} = \frac{B_{24}(\alpha^2 + B_{25}(-B_{27}) + B_{26}(B_{27})^2)}{(-B_{27})(B_{28} - B_{27})}, v$$

$$B_{31} = \frac{B_{24}(\alpha^2 + B_{25}(-B_{28}) + B_{26}(-B_{28})^2)}{(-B_{28})(B_{27} - B_{28})}, B_{32} = \frac{1 - \alpha}{G - \alpha + 1}, B_{33} = \frac{\alpha}{G - \alpha + 1}$$

$$f * g - \text{convolution of } f \text{ \& } g, f * g = \int_0^t f(z)g(t - z)dz$$